Research Article | Vol. 26, No. 1 | 8 Jan 2018 | OPTICS EXPRESS 488

Optics EXPRESS

Comparing laser induced plasmas formed in diode and excimer pumped alkali lasers

Aram H. Markosyan[1,2,*]

[1] *Sandia National Laboratories, Scalable Modeling & Analysis, Livermore, CA 94550, USA*
[2] *Department of Electrical Engineering and Computer Science, University of Michigan, Ann Arbor, 48109-2122, USA*
[*] *amarkos@sandia.gov*
www.markosyanaram.com

Abstract: Lasing on the D_1 transition ($6^2P_{1/2} \rightarrow 6^2S_{1/2}$) of cesium can be reached in both diode and excimer pumped alkali lasers. The first uses D_2 transition ($6^2S_{1/2} \rightarrow 6^2P_{3/2}$) for pumping, whereas the second is pumped by photoexcitation of ground state Cs-Ar collisional pairs and subsequent dissociation of diatomic, electronically-excited CsAr molecules (excimers). Despite lasing on the same D_1 transition, differences in pumping schemes enables chemical pathways and characteristic timescales unique for each system. We investigate unavoidable plasma formation during operation of both systems side by side in $Ar/C_2H_6/Cs$.

OCIS codes: (140.2180) Excimer lasers; (140.2020) Diode lasers; (140.5560) Pumping; (020.5780) Rydberg states; (260.3230) Ionization; (350.5400) Plasmas.

References and links

1. W. F. Krupke, R. J. Beach, V. K. Kanz, and S. A. Payne, "Resonance transition 795-nm rubidium laser," Opt. Lett. **28**(23), 2336–2338 (2003).
2. B. V. Zhdanov, T. Ehrenreich, and R.J. Knize, "Highly Efficient Optically Pumped Cesium Vapor Laser," Opt. Commun. **260**(2), 696–698 (2006).
3. Y. Wang, T. Kasamatsu, Y. Zheng, H. Miyajima, H. Fukuoka, S. Matsuoka, M. Niigaki, H. Kubomura, T. Hiruma, and H. Kan, "Cesium vapor laser pumped by a volume-Bragg-grating coupled quasi-continuous-wave laser-diode array," Appl. Phys. Lett. **88**, 141112 (2006).
4. W. F. Krupke, J. B. Raymond, K. K. Vernon, A. P. Stephen, and T. E. James, "New class of cw high-power diode-pumped alkali lasers (DPALs)," Proc. SPIE **5448**, 7–17 (2004).
5. A. H. Markosyan and M. J. Kushner, "Plasma formation in diode pumped alkali lasers sustained in Cs," J. Appl. Phys. **120**, 193105 (2016).
6. A. H. Markosyan, "On the importance of electron impact processes in excimer pumped alkali laser induced plasmas," Opt. Lett. **42**(21), 4295–4298 (2017).
7. R. M. Measures, "Electron density and temperature elevation of a potassium seeded plasma by laser resonance pumping," J. Quant. Spect. Rad. Trans. **10**, 107 (1970).
8. C. Vadla, V. Horvatic, D. Veza, and K. Kiemax, "Resonantly laser induced plasmas in gases: The role of energy pooling and exothermic collisions in plasma breakdown and heating," Spect. Acta B **65**, 33–45 (2010).
9. Q. Zhu, B. Pan, L. Chen, Y. Wang, and X. Zhang, "Analysis of temperature distributions in diode-pumped alkali vapor lasers," Opt. Commun. **283**(11), 2406 (2010).
10. R. J. Beach, W. F. Krupke, V. K. Kan, and S. A. Payne, "End-pumped continuous-wave alkali vapor lasers: Experiment, model, and power scaling," J. Opt. Soc. Am. B **21**, 2151 (2004).
11. B. V. Zhdanov, A. Stooke, G. Boyadjian, A. Voci, and R.J. Knize, "Optically pumped cesium-Freon laser," Opt. Express **16**, 748 (2007).
12. Ty. A. Perschbacher, D. A. Hostutler, and T. M. Shay, "High-efficiency diode-pumped rubidium laser: experimental results," Proc. SPIE **6346**, 634607 (2007).
13. B. V. Zhdanov, A. Stooke, G. Boyadjian, A. Voci, and R.J. Knize, "Rubidium vapor laser pumped by two laser diode arrays," Opt. Lett. **33**, 414 (2008).
14. B. D. Barmashenko, S. Rosenwaks, and M. C. Heaven, "Static diode pumped alkali lasers: Model calculations of the effects of heating, ionization, high electronic excitation and chemical reactions," Opt. Commun. **292**, 123 (2013).
15. A. D. Palla, D. L. Carroll, J. T. Verdeyen, J. D. Readle, T. M. Spinka, C. J. Wagner, J. G. Eden, and M. C. Heaven, "Multi–Dimensional Modeling of the XPAL System," Proc. SPIE **7581**, 75810L (2010).
16. A. D. Palla, J. T. Verdeyen, and D. L. Carroll, "Exciplex pumped alkali laser (XPAL) modeling and theory," Proc. SPIE **7751**, 77510F (2010).

#307850 https://doi.org/10.1364/OE.26.000488
Journal © 2018 Received 25 Sep 2017; revised 21 Dec 2017; accepted 22 Dec 2017; published 5 Jan 2018

Optics EXPRESS

17. A. D. Palla, D. L. Carroll, J. T. Verdeyen, and M. C. Heaven, "XPAL modeling and theory," Proc. SPIE **7915**, 79150B (2011).
18. A. H. Markosyan, A. Luque, F. Gordillo-Vazquez, and U. Ebert, "PumpKin: A tool to find principal pathways in plasma chemical models," Comp. Phys. Comm. **185**, 2697–2702 (2014).
19. A. H. Markosyan, A. Luque, F. Gordillo-Vazquez, and U. Ebert, "PumpKin: A tool to find principal pathways in plasma chemical models," `www.pumpkin-tool.org` (2013).
20. D. S. Stafford, and M. J. Kushner, "$O_2(^1\Delta)$ Production in He/O_2 Mixtures in Flowing Low Pressure Plasmas," J. Appl. Phys. **96**, 2451 (2004).
21. O. Zatsarinny, K. Bartschat, N. Yu. Babaeva, and M. J. Kushner, "Electron collisions with cesium atoms–benchmark calculations and application to modeling an excimer-pumped alkali laser," Plasma Sources Sci. Technol. **23**, 035011 (2014).

1. Introduction

DPALs, first demonstrated in 2003 [1], are a type of optically pumped lasers which use inexpensive semiconductor diode lasers as a pump to alkali vapor. Lasing on the D_1(894.59 nm) transition of alkali atom by directly exciting the D_2(852.35 nm) transition by the pump radiation are discussed in various references [1–3]. Recent studies showed that Rb and K based DPALs have yielding efficiencies in excess of 50% [2, 4], while models predict efficiencies up to 90%.

XPALs provide an alternative approach to optically pumping alkali lasers by photo-association of alkali-rare gas atomic collision pairs. In the four-level XPAL pumping scheme, the CsAr($B^2\Sigma^+_{1/2}$) state, the blue satellite, is optically pumped by 837 nm pulses, which followed by the dissociation of CsAr($B^2\Sigma^+_{1/2}$) and population of Cs($6^2P_{3/2}$). The alternative pumping scheme, not discussed in present work, is pumping of weakly-bound CsAr($A^2\Pi_{3/2}$) state, the red satellite, by 853 nm pump pulse, which followed by the dissociation of CsAr($A^2\Pi_{3/2}$) and population of Cs($6^2P_{3/2}$).

In both systems the $^2P_{3/2}$ states are further collisionally quenched to the $^2P_{1/2}$ state. Lasing occurs on the $^2P_{1/2} \rightarrow {}^2S_{1/2}$ transition, which requires the upper laser level to be inverted with respect to the ground state. During the operation of DPAL and XPAL a laser induced plasma is formed [5, 6]. One efficient mechanism for laser induced plasma is LIBORS (Laser Ionization Based on Resonance Saturation) proposed by Measures [7], according to which the electron heating by superelastic relaxation of laser-produced excited species then rapidly avalanches to nearly full ionization. Laser induced plasma can potentially decrease the laser performance. Other factors affecting the laser performance are the gas heating and rarefication of the laser medium [8–17]. The semi-analytical model developed by Barmashenko *et al.* exhibited a laser power increase during high power pumping of flowing gas DPALs by convective cooling [14]. Palla et al. and Carrol *et al.* have developed global and multidimensional models for XPALs in the Ar/Cs system [15–17]. They found that the increase in the cell temperature and Cs vapor pressure increases the XPAL efficiencies. Computational investigation of Cs/Ar XPALs conducted by Zatsarinny *et al.* revealed that 4 ns (3 μs inter-pulse period) 32 MW/cm^2 pulses produce electron densities exceeding the values of 10^{14} cm^{-3}, which ultimately reduces laser power by depletion of the ground state through ionization and by electron collision mixing of the laser levels [21].

In present paper, we discuss results from a computational investigation of the DPAL and XPAL systems in Ar/Cs/C_2H_6 mixture with lasing oscillations on D_1(894.59 nm) transition, Cs($6^2P_{1/2}$)$\rightarrow$ Cs($6^2S_{1/2}$). Our focus in this study was a side by side comparison of the mechanisms of the laser induced plasma formation in DPAL and XPAL. A weakly ionized plasma is formed and has the electron densities up to 10^{14} cm^{-3}. The dominant reactions underling in our analysis are obtained by the post-processing PumpKin tool [18, 19]. The global model used in the present work is described in section 2. Pumping two regimes of continuous wave (CW) and pulsed form, are discussed in sections 3 and 4. Our conclusions and remarks are made in section 5.

Optics EXPRESS

2. Description of the model

In this computational investigation we used Global_Kin, a global plasma kinetics model described in [20], where the rate equations for species densities, temperatures, pump intensities, and laser intensities are integrated as a function of time over successive pulsed periods. Electron impact processes are included in Global_Kin for elastic and inelastic collisions, including electronic and vibrational excitations, super-elastic collisions, ionization and recombination. The coefficients are obtained from solutions of Boltzmann's equation for the electron energy distribution function and are functions of electron temperature, which is the solution of the electron energy conservation equation.

The gas mixture of $Ar/C_2H_6/Cs = 85/15/1.8 \times 10^{-5}$ at 600 Torr pressure sustained in a cell at temperature of 425 K. We chose the initial electron density to be 10^6 cm^{-3}. The steady state (or pulsed-periodic steady state) electron density is not sensitive to the initial value. The initial Cs/Cs_2 densities are calculated by the vapor pressure based on the temperature of the laser cell, and are 2.4×10^{14} cm^{-3} for Cs and 2.4×10^{12} cm^{-3} for Cs_2. The cell used in this computational study is described in [21], which is 5 cm long resonator with a rear mirror having 100% reflectivity and output coupler with 98% reflectivity for the laser wavelength. Laser is pumped longitudinally with a single pass of the pump beam.

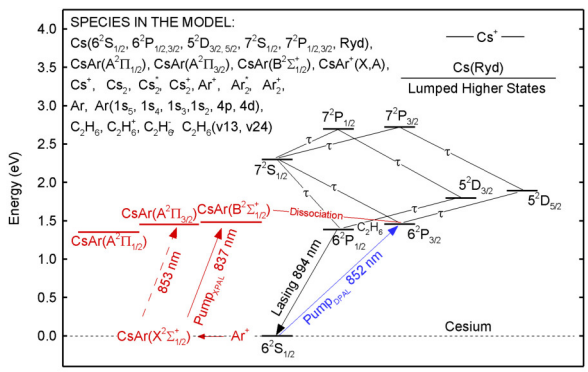

Fig. 1. Energy level diagram for cesium (Cs), DPAL and XPAL pumping schemes.

We have considered 629 reactions among the following species: e, $Cs(6^2S_{1/2}, 6^2P_{1/2}, 6^2P_{3/2}, 5^2D_{3/2}, 5^2D_{5/2}, 7^2S_{1/2}, 7^2P_{1/2}, 7^2P_{3/2}$, Ryd), Cs^+, Cs_2, $Cs_2{}^+$, $Cs_2{}^*$, Ar, $Ar_2{}^*$, Ar^+, $Ar_2{}^+$, $Ar(1s_5, 1s_4, 1s_3, 1s_2$, 4p, 4d), $CsAr(A^2\Pi_{1/2}, A^2\Pi_{3/2}, B^2\Sigma^+_{1/2})$, $CsAr^+$(X, A), C_2H_6, C_2H_6(v13, v24), $C_2H_6{}^+$, $C_2H_6{}^-$. Also, we included the diode laser pump intensity, φ_p, and laser intensities for the $Cs(6^2P_{1/2}) \rightarrow Cs(6^2S_{1/2})$ transition, φ_1(894.59 nm) and the $Cs(6^2P_{3/2}) \rightarrow Cs(6^2S_{1/2})$ transition, φ_2(852.35 nm). The electron impact cross sections for Cs were calculated using fully relativistic all-electron B-spline R-matrix (BSR) with pseudo-states ansatz with 311 coupled states.

In Fig. 1 we show the energy levels of Cs atom with allowed spectroscopic transitions between the excited states. In DPAL, pumping occurs at D_2(852.35 nm), on the $Cs(6^2S_{1/2}) \rightarrow Cs(6^2P_{3/2})$ transition and lasing occurs on the D_1(894.59 nm) transition, $Cs(6^2P_{1/2}) \rightarrow Cs(6^2S_{1/2})$. Collisional mixing (spin orbit relaxation) of the $^2P_{3/2}$ and $^2P_{1/2}$ levels is the key part of this three-level (in fact, a quasi-two-level) laser scheme. During the spin-orbit relaxation an electron in the $^2P_{3/2}$ state is relaxed to $^2P_{1/2}$ state through inelastic collisions with a ethane, while the energy difference between the ^2P levels is transferred to translational, rotational or vibrational modes of ethane or the translational energy of the Cs atom. Importantly, ethane has relatively large mixing rate (cross section) and small quenching rates of the ^2P levels.

As shown in Fig. 1, in XPAL pumping scheme, the $CsAr(B^2\Sigma^+_{1/2})$ state is optically pumped by

Optics EXPRESS

837 nm pulses, followed by the dissociation of $CsAr(B^2\Sigma^+_{1/2})$ state and population of $Cs(6^2P_{3/2})$. Once the $Cs(6^2P_{3/2})$ excited state is populated, the lasing is achieved by the same mechanism as for DPAL described above.

3. Continuous wave pumping regime

3.1. DPAL

In Fig. 2(a) we show the densities of species responsible for lasing for a CW DPAL pumping of Cs cell at the temperature of 425 K with a pumping power of 12 kW/cm^2. The pump at 852 nm depletes the population of the ground state cesium $Cs(6^2S_{1/2})$ into the $Cs(6^2P_{3/2})$ excited state. Then ethane collisionally relaxes the $Cs(6^2P_{3/2})$ into the $Cs(6^2P_{1/2})$ state. When the $Cs(6^2P_{1/2})$ state is sufficiently populated (1×10^{14} cm^{-3}), and the upper and lower laser levels are the same (determined by the ratio of the degeneracies), the intensity of the laser oscillation on the $Cs(6^2P_{1/2}) \rightarrow Cs(6^2S_{1/2})$ transition (894 nm) increases. After reaching threshold, laser oscillation and the densities of laser levels heavily saturate. The 6^2P states quenched in $ArCs^*$ dimer formation reactions with the following reaction rates:

$$Cs(6^2P_{3/2}) + Ar + M \rightarrow CsAr(A^2\Pi_{3/2}) + M \quad 1 \times 10^{-32} cm^6 s^{-1}, \tag{1}$$

$$Cs(6^2P_{3/2}) + Ar + M \rightarrow CsAr(B^2\Sigma^+_{1/2}) + M \quad 1 \times 10^{-32} cm^6 s^{-1}, \tag{2}$$

$$Cs(6^2P_{1/2}) + Ar + M \rightarrow CsAr(A^2\Pi_{1/2}) + M \quad 2 \times 10^{-32} cm^6 s^{-1}, \tag{3}$$

where M is a third body.

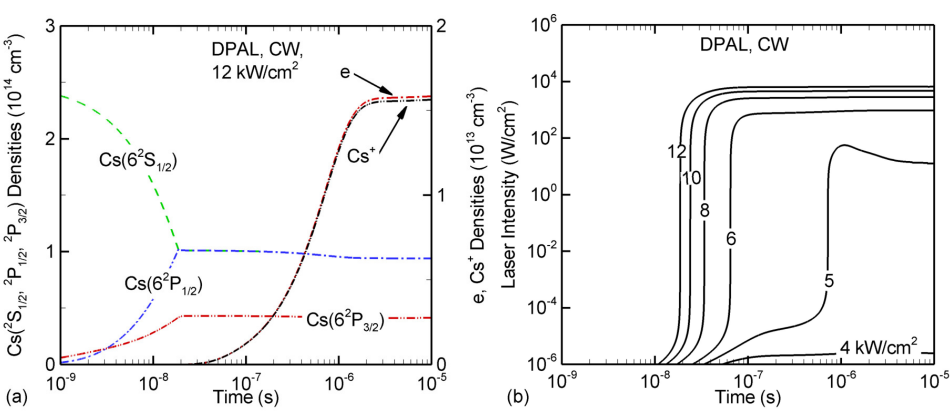

Fig. 2. (a) Density of species responsible for lasing during the first 10 μs of CW pumping for DPAL at 425 K, $[C_2H_6]$ = 0.15, 600 Torr. (b) Output laser intensity (894 nm) as a function of input pump powers of 4 - 12 kW/cm^2.

Besides $ArCs^*$ dimer formation reactions, the laser lower level $Cs(6^2S_{1/2})$ is quenched in the energy pooling reactions $[Cs(6^2S_{1/2}) + Cs(6^2S_{1/2}) \rightarrow Cs + Cs(7^2P_{1/2,3/2})]$ populate the upper $Cs(7^2P)$ states with a rate coefficient of 7×10^{-10} cm^{3}s^{-1}. The other energy pooling reactions populate cesium Rydberg states $[Cs^* + Cs^* \rightarrow Cs + Cs(Ryd)]$ with a rate coefficient of 1×10^{-10} cm^{3}s^{-1}. High intensity of laser radiation photoionizes the cesium 7^2S, 7^2P, and Rydberg states $[\varphi_1(894\text{ nm}) + Cs(7^2S, 7^2P, Ryd) \rightarrow Cs^+ + e]$ with a rate coefficient of 6×10^{-7} cm^{3}s^{-1} creating plasma densities of 1.6×10^{13} cm^{-3}, which corresponds to the fractional ionization of [e]/[Cs] = 0.06. The plasma consists of Cs^+ and $CsAr^+(X)$ ions, while latter is populated by the three-body

Optics EXPRESS

charge transfer reaction [$Cs^+ + Ar + M \rightarrow CsAr^+(X) + M$] with a rate coefficient of 5.6×10^{-32} cm^6s^{-1}. On the other hand, $CsAr^+(X)$ ions can populate the Cs^+ ions by the two-body charge transfer reaction [$CsAr^+(X) + Ar \rightarrow Ar + Cs^+ + Ar$] with a rate coefficient of 5.3×10^{-10} cm^3s^{-1}, with excess energy going to the gas heating.

Electron impact processes play a crucial role in mixing the 7^2S, 7^2P, and Rydberg Cs states. When the electron impact process increases the excitation level [$e_{hot} + Cs^* \rightarrow Cs^{**} + e_{cold}$], the electron loses its energy, while in the opposite case the electron gains the energy. The cesium excited states higher than 7^2S depleted by either spontaneous emission [$Cs^{**} \rightarrow Cs^* + \varphi$] or by the electron impact superelastic reactions [$e_{cold} + Cs^{**} \rightarrow Cs^* + e_{hot}$] increasing the electron temperature. The excitation transfer between excited states of cesium and ethane populates vibrational levels of ethane, which can causes an increase in gas temperature.

DPAL laser intensities for the input pump powers of 4 - 12 kW/cm^2 are shown in Fig. 2(b) as a function of time. When the pump power is low, it is not sufficient to produce a population inversion necessary for lasing. But when the pump power is higher than a certain threshold (in this case, the threshold is somewhere between 5 to 6 kW/cm^2) the laser upper level is high enough to produce lasing action. Increasing pump power will saturate the output laser intensity, as the pump rate is limited by the Cs vapor density and the maximum inversion density possible to achieve. Moreover, the time required to achieve a population inversion and start lasing is decreasing with increase of input pump power.

3.2. XPAL

In Fig. 3(a) we show the densities of species responsible for lasing for a CW XPAL pumping of Cs cell at the temperature of 425 K with a pumping power of 0.5 MW/cm^2. The pump at 837 nm populates the $CsAr(B^2\Sigma^+_{1/2})$ dimer by the following reaction:

$$\varphi_p(837\text{ nm}) + Cs(6^2S_{1/2}) + Ar \rightarrow CsAr(B^2\Sigma_{1/2}) \quad 6 \times 10^{-26} cm^6s^{-1}, \tag{4}$$

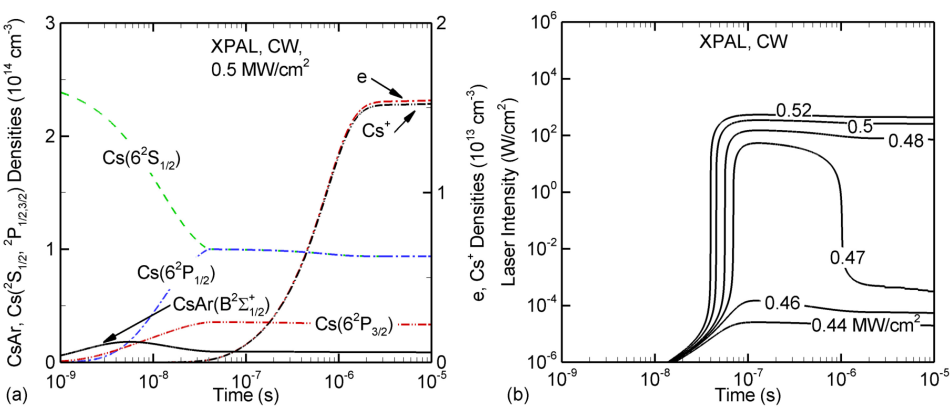

Fig. 3. (a) Density of species responsible for lasing during the first 10 μs of CW pumping for XPAL at 425 K, [C_2H_6] = 0.15, 600 Torr. (b) Output laser intensity (894 nm) as a function of input pump powers of 0.44 - 0.52 MW/cm^2.

Furthermore, the excited state $CsAr(B^2\Sigma^+_{1/2})$ gets dissociated and converted to the $Cs(6^2P_{3/2})$ excited state by the [$CsAr(B^2\Sigma^+_{1/2}) + M \rightarrow Cs(6^2P_{3/2}) + Ar + M$], where M is the third body, reaction with a rate coefficient of 2.1×10^{-10} cm^3s^{-1}. Once, the $Cs(6^2P_{3/2})$ state is populated,

Optics EXPRESS

the process resulting into the lasing are the same as for the DPAL's case: ethane collisionally relaxes the $Cs(6^2P_{3/2})$ into the $Cs(6^2P_{1/2})$ state and when sufficient density of $Cs(6^2P_{1/2})$ state is reached (1×10^{14} cm^{-3}), and the upper and lower laser levels are the same (determined by the ratio of the degeneracies), the intensity of the laser oscillation on the $Cs(6^2P_{1/2}) \rightarrow Cs(6^2S_{1/2})$ transition (894 nm) increases up to reaching a threshold, after which laser oscillation and the densities of laser levels heavily saturate. The mechanisms of formation of 7^2S, 7^2P, and Rydberg states in case of XPAL are the same as for DPAL laser. Unlike in DPAL, in XPAL the Cs upper states are photoionized by the intra-cavity pump radiation [φ_{intra}(837 nm) + Cs(7^2S, 7^2P, Ryd) $\rightarrow$ Cs^+ + e] with a rate coefficient of 6×10^{-7} cm^{3}s^{-1}.

One clear difference between the XPAL and DPAL lasers is that the former requires much higher (two orders of magnitude higher) pumping power and, despite of that, the lasing starts much later compared to the DPAL. The reason is that in XPAL the pumping is a three-body reaction, and hence, requires more time and pumping power to sufficiently populate the $CsAr(B^2\Sigma^+_{1/2})$, while in DPAL the $Cs(6^2P_{3/2})$ states are populated directly from the pump radiation. The plasma formation in both of the lasers is due to the photoionization of upper Cs states by laser radiation in the case of DPAL and by the intra-cavity pump radiation in the case of XPAL.

4. Pulse pumping regime

In this section we investigate both lasers when pumping power delivered in pulsed form. We identify two pulsing regimes: 1. low frequency regime, where the pump repetition frequency is 1 kHz and pump duration is 1 μs; 2. high frequency regime, where the pump repetition frequency is 1 MHz and pump duration is 10 ns. All the densities are built on pulse to pulse basis and achieve a pulse-periodic steady state in tens of successive pulses.

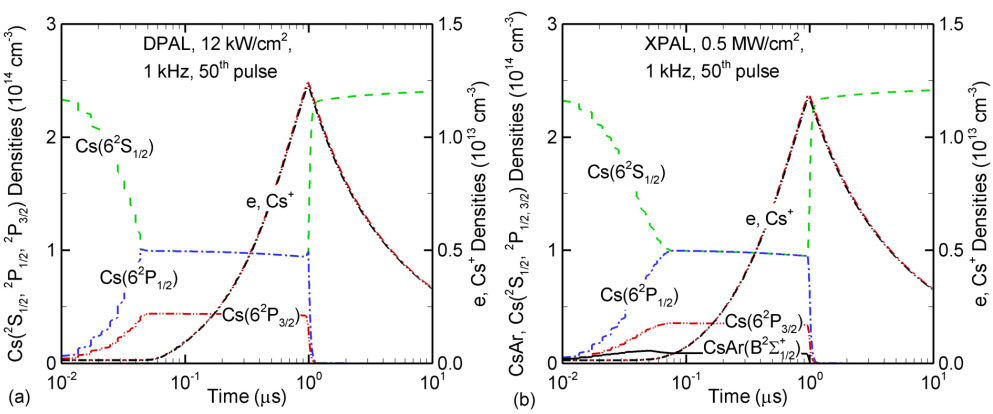

Fig. 4. Densities of species responsible for lasing at low frequency (1 kHz) pumping of (a) DPAL and (b) XPAL. The results are at 50th pulse.

The densities of electrons and cesium species as a function of time are shown for DPAL in Fig. 4(a) and for XPAL in Fig. 4(b) for the low frequency regime. In comparison with the constant wave (CW) form, in the pulsed case the densities are decreasing during the inter-pulse period when power is off. These low densities are just enough for the pump radiation to start with and produce the population inversion and lasing. The lasing mechanism, as well as the mechanism of plasma formation, in pulsed case is the same as in the CW case.

We show the densities of electrons and cesium species as a function of time are shown for DPAL in Fig. 5(a) and for XPAL in Fig. 5(b) for the high frequency regime. Due to very short

Optics EXPRESS

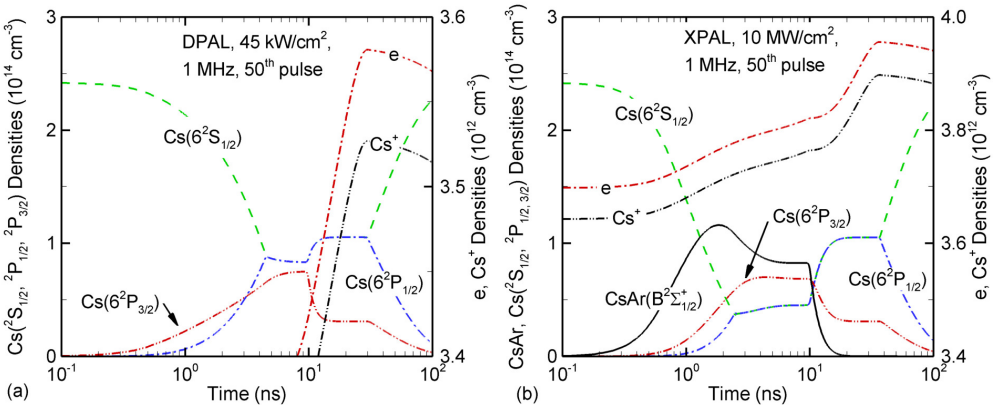

Fig. 5. Densities of species responsible for lasing at high frequency (1 MHz) pumping of (a) DPAL and (b) XPAL. The results are at 50th pulse.

pulse length we need much high pulse power to produce population inversion and lasing. As it was in all previous cases, the electron temperature is only slightly increased, but still it is too low to enable any electron impact reaction increasing the excitation from Cs(6^2P) state to populate the higher excited states.

When the pulse is off, in DPAL ethane continuous a depletion of Cs($6^2P_{3/2}$) and population of Cs($6^2P_{1/2}$) allowing lasing intensity to vanish slowly. In XPAL, the depletion of the large reservoir of CsAr($B^2\Sigma^+_{1/2}$) continuous dissociation and population of Cs($6^2P_{3/2}$) which then is transferred to the Cs($6^2P_{1/2}$) states. The mechanisms of formation of 7^2S, 7^2P, and Rydberg states in this case is the same as in all the previous cases, while the photoionization in XPAL is now sustained not by the intra-cavity pump radiation (which is gone with pulse power), but with φ_1(894 nm) laser radiation.

In Fig. 6 we show the 894 nm laser intensities as function of input pump power for both types of lasers pumped at low and high pump frequencies. In DPAL the pump power directly goes into the depletion of the ground state of cesium and population of Cs($6^2P_{3/2}$) state, while in XPAL the population of Cs($6^2P_{3/2}$) requires a three body-reaction (in general, a slow process) to populate the CsAr($B^2\Sigma^+_{1/2}$) and, then, dissociation of CsAr($B^2\Sigma^+_{1/2}$) into the Cs($6^2P_{3/2}$). This is the reason that DPAL is much more effective than XPAL. For the fixed pulse intensity, a higher energy per pulse is delivered by the lower frequency due to the longer pulse length. As a result, the lower the frequency the higher the laser intensities. In terms of energy per pulse, both systems are more efficient with higher frequency pulses.

5. Conclusion

We conducted a computational investigation of lasing performances of DPAL and XPAL systems sustained in Ar/C_2H_6/Cs mixture (425 K, 600 Torr) with lasing on the Cs($6^2P_{1/2} \rightarrow 6^2S_{1/2}$) (894 nm) transition. We concluded that during the operations of both lasers the plasma formation is unavoidable. Under the conditions considered in the present study, the plasma is formed by the photoionization of the 7^2S, 7^2P, and Rydberg states, which are populated from the Cs(6^2P) states by the energy pooling reactions. In XPAL, the intra-cavity pump radiation is primarily responsible for the photoionization, while in DPAL, the laser intensity produces photoionization.

Optics EXPRESS

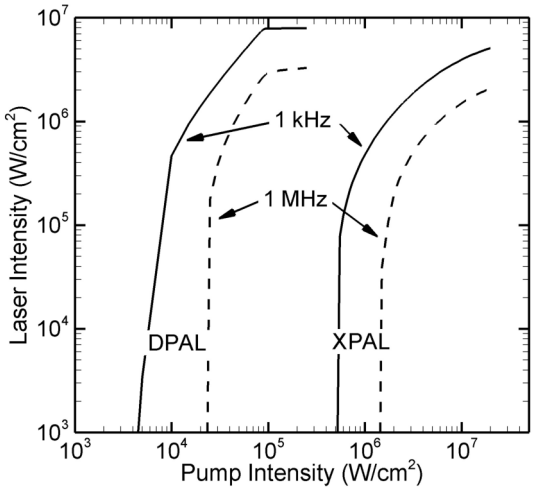

Fig. 6. 894 nm laser intensity for DPAL and XPAL as a function of pump intensity for 1 kHz and 1 MHz pump frequencies.

Funding

Sandia National Laboratories is a multimission laboratory managed and operated by National Technology and Engineering Solutions of Sandia, LLC, a wholly owned subsidiary of Honeywell International, Inc., for the U.S. Department of Energy's National Nuclear Security Administration under contract DE-NA0003525.

Acknowledgments

We thank Professor Mark J. Kushner for valuable discussions. This work was supported by the Department of Defense High Energy Laser Multidisciplinary Research Initiative.

Disclosures

'The authors declare that there are no conflicts of interest related to this article.